THE JOURNAL OF PHYSICAL CHEMISTRY Letters

Letter

Cite This: J. Phys. Chem. Lett. 2020, 11, 387−394

pubs.acs.org/JPCL

Exciton, Biexciton, and Hot Exciton Dynamics in $CsPbBr_3$ Colloidal Nanoplatelets

Brener R. C. Vale,[†,§] Etienne Socie,[†] Andrés Burgos-Caminal,[†] Jefferson Bettini,[‡] Marco A. Schiavon,[§] and Jacques-E. Moser*[,†]

[†]Photochemical Dynamics Group, Institute of Chemical Sciences & Engineering, École Polytechnique Fédérale de Lausanne, CH-1015 Lausanne, Switzerland

[§]Grupo de Pesquisa Química de Materiais, Departamento de Ciências Naturais, Universidade Federal de São João Del-Rei, Campus Dom Bosco, 36301-160 São João Del-Rei, Minas Gerais, Brazil

[‡]Laboratório Nacional de Nanotecnologia, Centro Nacional de Pesquisa em Energia e Materiais, Campinas, 13083-970 São Paulo, Brazil

Supporting Information

ABSTRACT: Lead halide perovskites have emerged as promising materials for light-emitting devices. Here, we report the preparation of colloidal $CsPbBr_3$ nanoplatelets ($3 \times 4 \times 23$ nm^3) experiencing a strong quasi-one-dimensional quantum confinement. Ultrafast transient absorption and broadband fluorescence up-conversion spectroscopies were employed to scrutinize the carrier and quasiparticle dynamics and to obtain a full description of the spectroscopic properties of the material. An exciton binding energy of 350 meV, an absorption cross section at 3.2 eV of $5.0 \pm 0.3 \times 10^{-15}$ cm^{-2}, an efficient biexciton Auger recombination lifetime of 9 ± 1 ps, and a biexciton binding energy of 74 ± 4 meV were determined. Moreover, a short-lived emission from hot excitons was observed, which is related to the formation of band-edge excitons. The time constant of both processes is 300 ± 50 fs. These results show that $CsPbBr_3$ nanoplatelets are indeed quite promising for light-emitting technological applications.

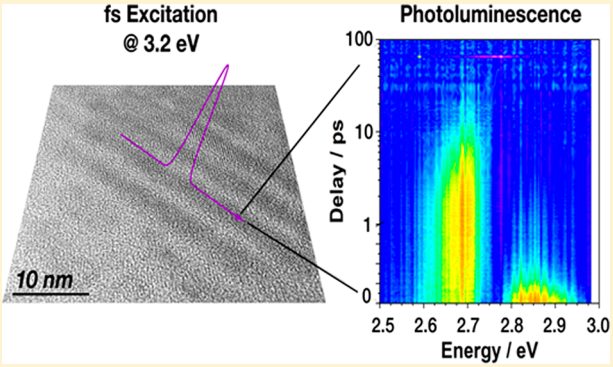

Metal halide perovskite (MHP) materials have been the object of intense research in the past decade since their first application in photovoltaic cells in 2009.[1] Currently, the best efficiency for perovskite solar cells exceeds 25%.[2] Beyond photovoltaic applications, perovskites have been applied in different technological devices, such as LEDs,[3,4] lasers,[5] and photodetectors,[6] as well as photocatalytic materials for organic synthesis.[7] Perovskites possess many interesting properties, such as a high photoluminescence quantum yield, extended carrier lifetime, and long charge diffusion lengths. Because of their versatility, distinct perovskite compositions and nanostructures with or without quantum confinement effects have been studied, such as quantum dots (QDs) (0D), nanorods (NRs) (1D), and nanoplatelets (NPls) (2D).[8,9] Quantum confinement effects increase the exciton binding energy and exciton radiative recombination, making these materials more interesting for LEDs and laser devices than the bulk analogues. In contrast, bulk compounds are better suited for photovoltaic applications, where an efficient charge separation is required.[10] Studies on the bulk form of perovskites have shown that they have a slow hot-carrier relaxation, ∼1 ps, which can help increase the carrier diffusion length, resulting in better efficiency.[10−12] However, LEDs require fast hot-carrier dynamics because of the competition between hot-carrier relaxation and charge-trapping dynamics.[10] Multiexciton recombination through nonradiative Auger recombination, in which an exciton transfers its energy to a third particle, exciting it into a higher state, competes with both processes of exciton radiative recombination and charge separation. Furthermore, the Auger recombination probability increases with quantum confinement because the momentum conservation requirement is relaxed.[13] Another parameter strongly dependent on the quantum confinement is the biexciton binding energy; a biexciton consists of two neutral bound excitons red-shifted compared to the unbound excitons because of Coulombic effects. Nagamine et al. demonstrated a strong correlation between the biexciton binding energy and amplified spontaneous emission (ASE) threshold in perovskite nanocrystals (NCs).[14] Although many studies on ultrafast processes, such as biexciton Auger recombination, ASE, and carrier relaxation dynamics, have been conducted in recent years, they have

Received: November 6, 2019
Accepted: December 23, 2019
Published: December 23, 2019

DOI: 10.1021/acs.jpclett.9b03282
J. Phys. Chem. Lett. 2020, 11, 387−394

focused mainly on larger cubic NCs, which lie in the weak quantum confinement regime.[13,15−21] Recently, Rossi et al. showed that the presence of excitons can activate a forbidden transition in strongly confined perovskite QDs, which explains a particular feature in the transient absorption spectrum of perovskite NCs.[22] Li et al. reported the absence of a phonon bottleneck in strongly confined perovskite QDs.[23] Most of these studies were carried out using transient absorption spectroscopy (TAS). Although the hot exciton transition becomes more spaced in structures with strong quantum confinement,[22,24] directly detecting this process by TAS is difficult because of limitations on the white light probe beam and the complexity of the signal which can encompass ground-state bleaching, emission, and excited-state absorption. In this scenario, application of time-resolved fluorescence spectroscopy appears as an interesting alternative, as this technique allows us to monitor the population dynamics of the sole excited states. Here, we use femtosecond broadband fluorescence upconversion spectroscopy (FLUPS) for detecting hot exciton and biexciton emission. By gating the fluorescence with an ultrashort laser pulse, we are able to access the initial 0−1 ps time window with a flat spectral response, which allows single-scan pump-gate measurements for the entire visible spectrum.[25] Considering previous studies, we prepared very small colloidal nanoplatelets (CNPls) lying in the strong quantum confinement regime with a narrow size distribution and in the absence of different structures. We conducted a careful study combining both ultrafast techniques, TAS and FLUPS. We explored the dynamics of band-edge excitons at low and high fluences, the biexciton Auger recombination lifetime, the biexciton binding energy, and the hot exciton emission.

$CsPbBr_3$ CNPls were prepared at room temperature by a procedure described previously in the literature with some modifications. Details of the procedure are reported in the Supporting Information.[26] First, a stability test was performed in different solvents, such as hexane, dodecane, toluene, and chlorobenzene (Figure S1). Dodecane and hexane appeared as the best solvents for stabilizing the CNPls for a long period of time; however, the growth of the particles in dodecane was slower than that in hexane. Figure 1a shows a transmission

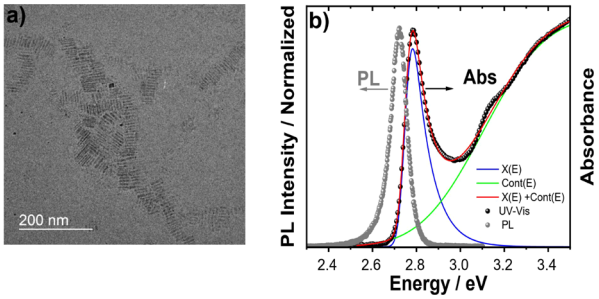

Figure 1. (a) Transmission electronic microscopy image of $CsPbBr_3$ CNPls. (b) Emission and absorption spectra (gray and black spheres), where the red line is the fitted model and the blue and green lines are the exciton and continuum contributions, respectively.

electron microscopy (TEM) image of the $CsPbBr_3$ CNPls. The particles have a rectangular shape with average lateral sizes of 4 ± 2 nm and length of 23 ± 7 nm (Figure S2). Figure 1b shows the emission and absorption spectra for $CsPbBr_3$ CNPls in hexane (Figure S3 displays the second-derivative spectrum for $CsPbBr_3$ CNPls). The absence of reverse peaks in the region between 460 and 550 nm indicates the absence of larger particles and of different shapes, such as cubic NCs. The emission and absorption spectra show very narrow and symmetric bands and a blueshift of approximately 420 meV compared to the bulk value of 2.36 eV.[27] The absorption peak is located at 2.78 eV (∼445 nm). The photoluminescence (PL) peaks at 2.72 eV (455 nm), with a Stokes shift of approximately 60 meV and an emission quantum yield of 30%. According to previous reports, the excitonic absorption at 2.78 eV corresponds to the band-edge transition of 5 monolayers of $CsPbBr_3$ with a thickness of ∼3 nm.[27,28] Hence, the shape of the nanoplatelets of dimensions 3 × 4 × 23 nm^3 approaches that of nanorods with a strong quasi-1D quantum confinement. The full-width at half-maximum (fwhm) of the PL band is 84 meV, which is narrower compared with that of other NPls (90−170 meV)[27,28] and cubic NCs (100−200 meV),[10,17,29,30] indicating uniform quantum confinement in the structure. We observed one strong and very well-shaped exciton transition and two weak ones in the absorption spectra, corresponding to the second and third exciton transitions of ∼3.1 and 3.36 eV, which could be better resolved in the photoluminescence excitation (PLE) spectrum (Figure S4). We observe an asymmetry on the emission spectrum of the CNPLs, which is typical for perovskites in a strong quantum confinement regime.[29,31] Time-resolved emission spectra (TRES) measured on the nanosecond time scale confirm that the shoulder does not result from the presence of different particle sizes (see Figure S5 and the related discussion). We used a well-known model for quantum wells to fit the steady-state absorption spectrum according to previously reported papers,[28,32] but we fitted only the first exciton transition because the contributions of the second and third transitions were not very pronounced. Basically, this model consists of the exciton and continuum absorption band contributions (see the Supporting Information for more details). We find a value of 350 ± 10 meV for the exciton binding energy (E_b), which is greater than the results for other NPls (120−260 meV)[28,32] and 1 order of magnitude greater than that for bulk $CsPbBr_3$ of ∼40 meV.[33] Theoretically, the enhancement in E_b for two-dimensionally confined excitons is four times. Because our calculation exceeds this value, it is concluded that the reduced lateral dimensions in the CNPls, especially the width, lead to strong quasi-1D quantum confinement and a large dielectric mismatch between the inorganic $CsPbBr_3$ and the organic environment of the ligands. A similar behavior was reported for CdSe nanorods.[34]

We applied TAS and FLUPS techniques to evaluate some photophysical processes that occur on an ultrafast time scale. Figure 2a shows the transient absorption spectra at different time delays, and Figure 2b shows a two-dimensional representation of the fluorescence upconversion spectra of the $CsPbBr_3$ NPls at a low fluence, with an average exciton occupancy per particle $\langle N_x \rangle$ of less than 0.3. In this regime, the probability of Auger recombination due to multiexcitons is negligible, and only exciton recombination is considered to occur. This assumption can be verified by the normalized transient absorption spectral shape (Figure S6), which is independent of the time delay between 1 and 1000 ps.

The TA spectra show a bleaching peak at 2.77 eV, labeled B1 in Figure 2a, close to the excitonic peak in the absorption spectrum, which is related to the state filling of band-edge excitons (electrons and holes), and two photoinduced absorption bands: A broad band at approximately 3.0 eV,

DOI: 10.1021/acs.jpclett.9b03282
J. Phys. Chem. Lett. 2020, 11, 387−394

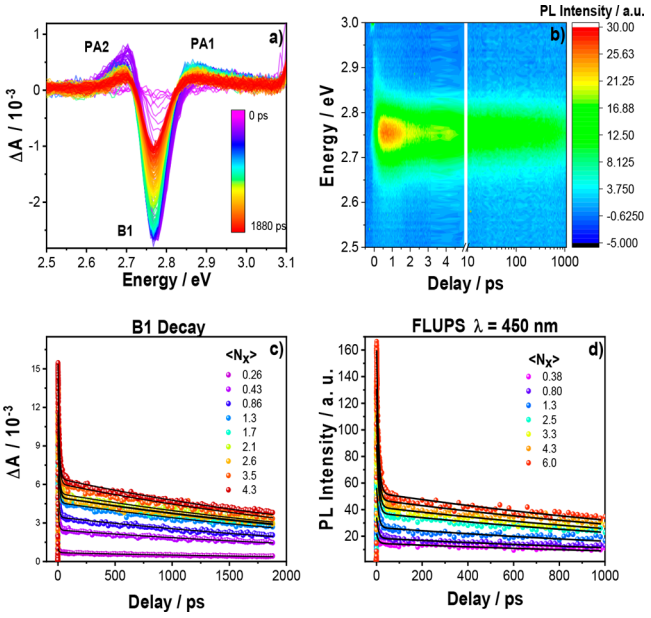

Figure 2. (a) Transient absorption spectra at different time delays at a low fluence. (b) Two-dimensional representation of FLUPS spectra at a low fluence. (c) B1 decay at different fluences. (d) Decay at 450 nm obtained by FLUPS at different fluences.

labeled PA1, was reported to be related to a forbidden exciton transition, which is activated by the presence of the band-edge excitons in strongly quantum confined QDs.[22] However, for weakly quantum-confined nanocrystals[13] and in bulk perovskites, this band has been assigned to band gap renormalization.[35] Another band centered at 2.70 eV, labeled PA2, is assigned to the Stark effect produced by the interaction between hot excitons and band-edge excitons.[22,23,36]

The second exciton transition is not observed in the TA spectra because it is resonant with the excitation energy. The upconversion photoluminescence spectrum shows an emission closely centered around the steady-state emission spectrum and one short-lived component at approximately 2.85 eV, which will be discussed later. Initially, we evaluated the dynamics of the bleaching feature B1 and the maximum of the upconversion photoluminescence over a longer time scale using different fluences of $0.26 \leq \langle N_x \rangle \leq 6$. As shown in Figure 2c,d, the dynamics is biexponential, with a short-lived component and a long component. The profile of the fluence-dependent decay is very different from those of bulk or quasi-2D perovskites, which follow the $1/\tau$ characteristic of the bimolecular recombination of free carriers.[11] The different behavior in the system studied here is expected owing to the high exciton binding energy, which avoids the dissociation of excitons into free carriers at room temperature.

The amplitude of the short-lived component increases when the photon fluence increases, which could be attributed to biexciton Auger recombination. We fitted the data from 1 to 1880 ps in TAS and until 1000 ps in FLUPS using a biexponential function. We observed that the time constant does not change very much with the fluence; only the amplitude is increased. We found time constants of 8.0 ± 2 ps for the short-lived component and greater than 2000 ps for the long component by both techniques (see the Supporting Information for the details of the fitting procedure).

The long decay measured by TAS and FLUPS is an extrapolation because our optical delay stages are limited to the range mentioned above. However, we could measure this decay by use of the time-correlated single-photon counting (TCSPC) technique, which gave two exponential decays with time constants of 2.3 ± 0.1 and 4.9 ± 0.1 ns (see Figure S7). The double-exponential PL decay behavior is attributed to exciton and trap-assisted recombination. We attribute the time constant decay of 4.9 ns to trap-assisted recombination because this process is characterized by a slow decay due to the accumulation of charges and slow depopulation. The good stoichiometry and the highly ionic nature of the perovskite is expected to yield practically no bulk point defects in nanoparticles. Trap sites involved in the latter process are, then, believed to result mainly from surface defects in a material characterized by a large surface/volume ratio.[31,32] The faster decay, which is closer to the values measured by FLUPS and TAS, is attributed to excitonic recombination.

To ascertain if the fast recombination comes from the biexcitons, we used a procedure based on Poisson statistics that is well-described in the literature.[13,15,37] The probability of having n excitons per particle is given by the Poisson statistics, as shown in eq 1:

$$P(n) = \frac{\langle N_x \rangle^n \cdot e^{-\langle N_x \rangle}}{n!} \tag{1}$$

where $\langle N_x \rangle$ is the average exciton occupancy per particle, which is also equal to the product of the absorption cross section of the CNPls measured at a specific excitation energy ($\sigma_{3.2.eV}$) and the density of photons per pulse per area (j): $\langle N_x \rangle = (\sigma_{3.2.eV}) \cdot j$. At the earlier time of 3 ps, each CNPl is populated at the band edge by up to two excitons because of the 2-fold degenerate edge. Those particles that have absorbed just one photon contribute only once to the signal, and all others that have absorbed more than one photon per pulse will contribute twice. After a long time delay, all biexcitons have already decayed via Auger recombination, and only one exciton occurs per particle independent of the initial number of excitons created. In this case, all CNPls will contribute just once to the bleaching, which can be modeled by eq 2:

$$\Delta A = A[1 - P(0)] = A(1 - e^{-\langle N_x \rangle}) \tag{2}$$

We can also define the TA bleaching for the biexciton as eq 3:

$$\frac{\Delta A}{A} = P(1) + 2[1 - P(0) - P(1)]$$
$$= A[2 - (2 + \langle N \rangle) \cdot e^{-\langle N_x \rangle}] \tag{3}$$

Figure 3a shows plots of the amplitude of the bleaching measured at the peak B1 in the TA spectra, at the later time

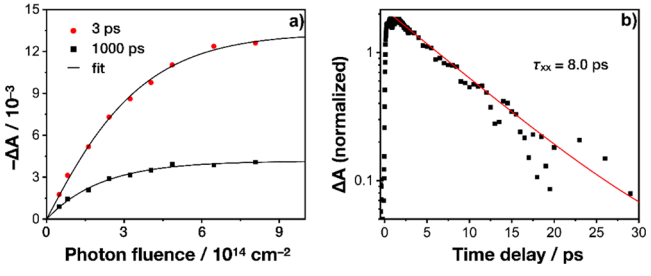

Figure 3. (a) Dependence of TA bleaching on the photon fluence at 3 and 1000 ps. (b) Biexciton Auger recombination lifetime.

DOI: 10.1021/acs.jpclett.9b03282
J. Phys. Chem. Lett. 2020, 11, 387−394

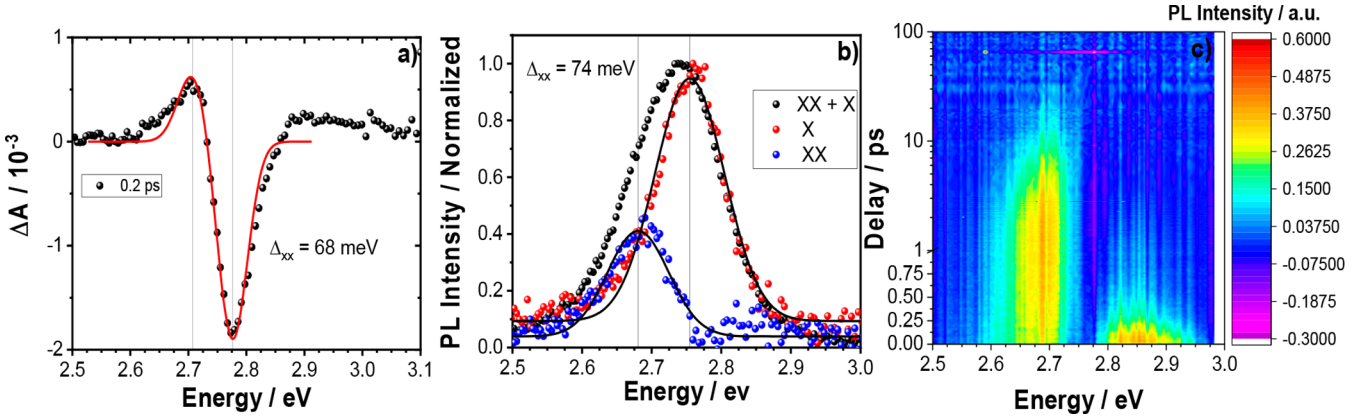

Figure 4. (a) Transient absorption spectrum at 0.2 ps. (b) FLUPS spectra at 1 ps (black dots) and 100 ps (red dots), and the biexciton emission spectrum obtained from the subtractive procedure (blue dots). (c) Two-dimensional representation of the reconstructed emission spectra obtained from the subtractive procedure from −0.1 to 100 ps.

delay of 1000 ps and earlier time delay of 3 ps, as a function of the fluence and fitted with eqs 2 and 3, respectively. When the fast component comes exclusively from biexcitons, both equations should be fitted with the same value of the cross section $\sigma_{3.2eV}$.[15] In this case, we found a figure $\sigma_{3.2eV} = 5.0 \pm 0.3 \times 10^{-15}$ cm^{-2}, which indicates that the fast component comes from biexciton Auger recombination. With the value of $\sigma_{3.2eV}$, we can estimate the $\langle N_x \rangle$ for the different photon fluences employed.

We also measured the biexciton Auger recombination lifetime. In this approach, we used the methodology described by Klimov et al.[37] Basically, we normalized the data at the longer time delay, and we subtracted the data at a high fluence from those at the lowest fluence (Figure S8). The result is a monoexponential decay (Figure 3b). We found time constants of 8.0 ± 0.3 ps with our data from TAS and 10.0 ± 0.5 ps when measured by FLUPS (Figure S9 shows a comparison between the decays obtained by TAS and FLUPS). The biexciton decay has two components: biexciton Auger recombination ($\tau_{xx,A}$) and biexciton radiative decay ($\tau_{xx,r}$). The latter is estimated to be one-fourth of the exciton radiative decay ($\tau_{x,r}$). We measured the exciton recombination decay, which is constituted by $\tau_{x,r}$ and the nonradiative decay ($\tau_{x,nr}$), as 2.3 ns. Thus, we can say that $\tau_{x,r}$ is <2.3 ns. Because we measured a biexciton recombination decay much smaller than 2.3 ns (8–10 ps), we can claim that biexciton Auger recombination dominates the biexciton decay.[38]

The biexciton Auger recombination rate increases when the overlap between the hole–electron pair wave functions increases. The value for the absorption cross section reported by Padilha et al. linearly depends on the volume of the cubic NCs from 0.34 to 15 × 10^{-15} cm^2, and they found a biexciton Auger recombination lifetime from 5 to 30 ps, which was sublinearly dependent on the absorption cross section, $\tau_{xx} = cV^{0.5}$. They concluded that this sublinear relation is due to the weak quantum confinement of the particles studied.[15] Recently, Li et al. demonstrated that biexciton Auger recombination for perovskite NCs has a linear relationship with the particle volume in the strong quantum confinement regime.[39] According to the latter report, for NCs of 280 nm^3, we should expect a biexciton Auger recombination lifetime of approximately 20 ps, twice as long as what we have found. This result indicates that the biexciton Auger recombination is more efficient in perovskite CNPls than in cubic NCs. Klimov's group showed that biexciton Auger recombination in PbSe nanorods (NRs) has a linear dependence on both the volume and absorption cross section.[37] They compared the absorption cross sections for NRs and QDs with the same volume and same band gap and found that the absorption cross section is three times larger for NRs than for QDs. Nevertheless, they also found that the local field correction factor, which accounts for incomplete penetration of the external field into NRs, is also three times larger for NRs than for QDs. As a result, the log–log plot of the biexciton Auger lifetime versus the absorption cross section shows similar values for both NRs and QDs.[40] Furthermore, Li et al. showed that the biexciton Auger lifetime in CdSe NPls does not follow the "universal volume scaling law"; instead, they found a linear scaling with the NPl area. Additionally, they showed that the NPl thickness plays an important role, and the thickness is proportional to the biexciton Auger lifetime. Finally, they concluded that the nonconfined dimension can be accounted for by the binary collision frequency for forming biexciton complexes, while the dependence on the quantum-confined dimension accounts for the Auger recombination probability of biexciton complexes.[41] Therefore, these studies demonstrate that this "universal volume scaling law" is not valid for semiconductors with different morphologies and compositions.

We expected different behavior for perovskite nanomaterials compared to PbSe or CdSe nanomaterials because the biexciton Auger lifetime in perovskites is much shorter than that in chalcogenide nanostructures.[15,37,39] This fact comes from the similarities between the effective masses of both electrons and holes in perovskites.[38] In CdSe, for example, biexciton Auger recombination is dominated by the excitation of electrons ($m_e = 0.13m_0$) because the excitation involving heavy holes is more difficult because of the greater effective mass ($m_h = 0.9m_e$).[38,41] Li et al. reported an interesting study on the size- and morphology-dependent Auger recombination in $CsPbBr_3$.[38] They obtained $CsPbBr_3$ NPls with lateral areas from 352 to 1104 nm^2 and NRs 3 nm in diameter with lengths from 43 to 84 nm. They found that the biexciton Auger lifetime does not have a linear dependence on the volume but on the lateral area for NPls or length for NRs.[38] Because our CNPls have a strong confinement in two dimensions (width and thickness), our results agree very well with the results for NRs reported by Li et al.[38]

DOI: 10.1021/acs.jpclett.9b03282
J. Phys. Chem. Lett. 2020, 11, 387–394

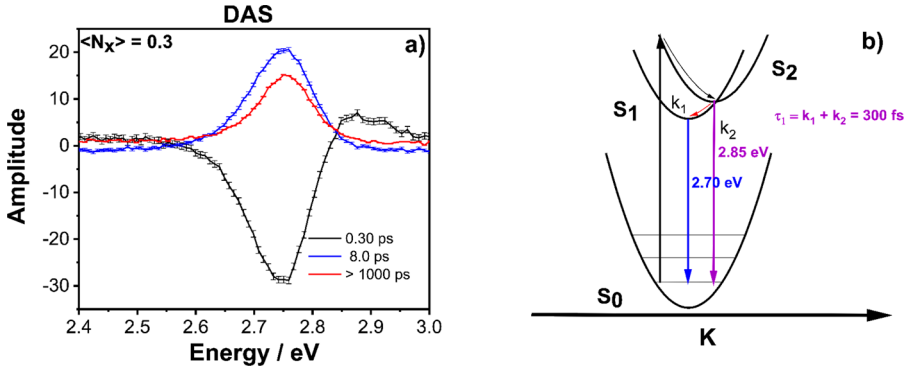

Figure 5. (a) Decay-associated spectra (DAS) obtained from FLUPS. (b) Scheme showing the mechanisms involved in hot exciton emission.

The TA spectrum is similar to the second derivative of the steady-state absorption spectrum. The short-lived PA2 spectral feature has been observed in different materials, such as II−VI QDs, and in perovskite materials, even in bulk or quantum-confined structures. This feature has been ascribed to the biexciton-induced Stark effect due to the shifting of the band-edge exciton absorption in the presence of the hot excitons created by the pump pulse. The Coulomb interaction between the excitons redshifts the exciton resonance, appearing in the spectrum as a bleaching at the resonance position of the first excitonic band and a photoinduced absorption at lower energy. This biexciton state decays very quickly, which is associated with the cooling of the hot excitons into the band-edge state. Therefore, this biexciton state has been used to study the carrier energy relaxation in traditional QDs and in perovskite materials.[42,43] We calculated the biexciton binding energy (Δ_{xx}) by fitting the TA spectrum at a 0.2 ps time delay with two Gaussian functions, as shown in eq 4. As suggested by Aneesh and colleagues, in the presence of a hot exciton, the transition energy of the probe excitons will be red-shifted by Δ_{xx}[44]

$$\Delta A(E) = A_1 \cdot \exp\left[-\left(\frac{E - E_X - \Delta_{xx}}{w}\right)^2\right] - A_2 \cdot \exp\left[-\left(\frac{E - E_X}{w}\right)^2\right] \quad (4)$$

where A_1 and A_2 are the amplitudes of PA2 and B1 features, respectively. Furthermore, E_X is the exciton transition energy, and w is the line width of the band-edge transition. Both parameters were obtained from fitting of the steady-state absorption spectra and were found to be 2.776 eV and 36 meV, respectively. Using this methodology, we found a value of Δ_{xx} of 68 ± 4 meV (Figure 4a). This value is greater than that of $CsPbBr_3$ NCs, 30 ± 5 meV, which lies in the weak quantum confinement regime.[44]

Although many studies have applied the methodology described above to calculate Δ_{xx} by TAS, Klimov and colleagues have shown that TAS is not the best way to measure this interaction energy in CdSe.[42] In this case, the biexciton comprises not only a well-defined $1S_u$ exciton (the 1S electron and the $1S_u$ hole) but also a poorly defined exciton in some highly excited state. For this case, the most direct approach to measure Δ_{xx} is based on the relative position of the exciton and biexciton emission bands, which can be measured by FLUPS. The radiative recombination of the biexciton produces a photon ($h\nu_{xx}$) and an exciton state (X), but this exciton could be in its excited or ground state. However, if we suppose that the biexciton decays into the ground-state single exciton E_x, then the shift of the biexciton will be given by $h\nu_{xx} = E_x + \Delta_{xx}$, which provides a direct measurement of Δ_{xx}.[42] Therefore, we employed fluence-dependent FLUPS to confirm the value of Δ_{xx} obtained from TAS (Figure S10 shows the two-dimensional representation of the FLUPS spectra at different photon fluences). When $\langle N_x \rangle$ is less than 1, the time-resolved spectra show a narrower emission and a homogeneous decay, while when $\langle N_x \rangle$ is greater than 1, the spectra become broader at earlier times and narrower after 10 ps. This broadening at earlier times is due to the emission from biexcitons, which decays readily via biexciton Auger recombination (the plot of Figure S11 confirms the quadratic behavior expect for the biexciton). Therefore, to calculate Δ_{xx} and obtain the biexciton emission spectra, we subtracted the emission spectrum at a high fluence from that at a low fluence, both at 1 ps; subtraction of a spectrum at high fluence at 1 ps from that at the same fluence at 100 ps, when the emission from the biexcitons has already decayed, could also be utilized. We compared both spectra and found that they are very similar; however, the signal-to-noise ratio is better for the spectrum taken at 100 ps at a high fluence (Figure S12 shows this comparison). Figure 4b shows the spectrum for $CsPbBr_3$ CNPls at a high fluence at 1 ps (black dots) when both excitons and biexcitons contribute to the emission spectrum (XX + X), the spectrum at 100 ps when the spectrum is composed only of the exciton recombination contribution (red dots), and the biexciton emission spectra (blue dots) obtained through the subtractive procedure. We also performed a Gaussian fit of the spectra to accurately measure the center of the band. Following this procedure, we measured a value of 74 ± 2 meV, which is statistically similar to the result obtained by TAS. The theoretical prediction indicates that the biexciton and exciton binding energies have a ratio of $\Delta_{xx}/E_b = 0.228$. Using our value of E_b = 350 ± 10 meV, we calculate Δ_{xx} to be 80 ± 4 meV, which is very close to the value experimentally measured by use of both FLUPS and TAS. Castañeda et al. showed that Δ_{xx} is dependent on the size of perovskite NCs, and they found values between 100 and 40 meV.[15] Recently, Ashner et al. showed that biexciton interaction in $CsPbBr_3$NCs in a weak confinement regime is repulsive and with energies increasing with decreasing size.[45] This finding is contradictory to the results presented by Castañeda et al. Ashner et al. used TAS combined with a method of target analysis to extract the component spectra corresponding to exciton and biexciton states. TAS has its limitations because of complexity of the signal, while Castañeda et al. used TRES, which was limited by the time resolution of their system (200 ps). In our case, the FLUPS

DOI: 10.1021/acs.jpclett.9b03282
J. Phys. Chem. Lett. 2020, 11, 387−394

spectrum is simple and the time resolution (<1 ps) is high enough to measure such processes. Therefore, we can say that in $CsPbBr_3$ CNPls, the exciton−exciton interaction in biexcitons is attractive. The large value of Δ_{xx} also indicates that the biexciton is stable at room temperature. Nagamine et al. showed a strong correlation between increasing Δ_{xx} and decreasing ASE threshold.[14] Therefore, we expect that $CsPbBr_3$CNPls will be a promising candidate for devices based on low-threshold ASE because of the high Δ_{xx} and larger absorption cross section compared to QDs.

We also performed the same procedure described above to isolate the biexciton emission, but with different time delays spaning from −0.1 to 98 ps, and the result is shown in Figure 4c. From this two-dimensional representation of the FLUPS spectra, the decay from the biexciton emission is clear. Moreover, a contribution from the hot excitons is observed, i.e., the emission at approximately 2.9 eV, which decays very quickly, within ∼0.3 ps. The emission of hot excitons occurs even at low fluences (Figure S8). To ascribe this ultrafast emission to a hot exciton, we used a global analysis of the FLUPS data (see the Supporting Information for details). Figure 5a shows a decay-associated spectrum (DAS) obtained by FLUPS. We observed an ultrafast component of 0.3 ± 0.05 ps, which manifests as a positive signal due to hot exciton emission and a negative signal due to the rise of the band-edge emission. The second contribution comes from the biexcitons at 8.0 ps, and the third contribution, which is greater than 2.0 ns, is due to exciton recombination (Figure S13 shows the DAS for different fluences). At high fluences, the biexciton contribution is larger and redshifts the spectra; however, the DAS at 8 ps has contributions from both exciton and biexciton emission. We observed that the decay for hot excitons is linked to the rise of the band edge. Because we have used an excitation energy of ∼3.1 eV, which is resonant with the second exciton transition, this state is populated and quickly relaxes, on a time scale close to the instrument response function (IRF) width of the experiment. In this scenario, excitons can be emitted from the edge of the second transition, producing hot exciton emission or decay via internal conversion to the first excited state, given the rise of the band-edge exciton emission, as shown in Figure 5b. Recently, Papagiorgis et al. reported that hot carriers in formamidinium lead iodide NCs decay very slowly, within ∼0.8 ns.

They also showed that under high fluence, $5 \leq \langle N \rangle \leq 10$, the emission from hot carriers is prolonged, which can delay the onset of the population inversion, suppressing the ASE in favor of the emission from hot excitons.[46,47] Therefore, because the hot exciton emission in our system is very fast, besides other properties discussed above, our colloidal suspension of nanoplatelets could be an interesting candidate for ASE.

In summary, we have synthesized minute CNPls (thickness = 3.0 nm, width = 4.0 ± 2 nm, and length = 23 ± 7 nm). This material shows a large blueshift in both the photoluminescence and absorption spectra compared with the bulk, with a larger exciton binding energy of approximately 350 meV. Using the ultrafast spectroscopy technique, we calculated that the absorption cross section of this material is $5.0 \pm 0.3 \times 10^{-15}$ cm^{-2} and that the biexciton Auger recombination lifetime is 9 ± 1 ps. Additionally, we showed that this kind of material does not follow the "universal scaling law" observed for II−VI−IV−VI QDs. We also calculated the biexciton binding energy (74 ± 2 meV) through two different techniques, which statistically gave the same results. Finally, we observed emission and decay from a hot exciton state (2.85 eV), which is linked with the rise of the band-edge emission. On the basis of these results, we expect that quasi-1D nanoplatelets, with their large biexciton binding energy, large absorption cross section, and ultrashort hot exciton emission, will be promising candidates for devices based on low-threshold ASE.

■ ASSOCIATED CONTENT

Supporting Information

The Supporting Information is available free of charge at https://pubs.acs.org/doi/10.1021/acs.jpclett.9b03282.

Methods, equation fitting, global analysis, quantum well model, stability in different solvents, TEM images, histogram for the length and width of $CsPbBr_3$, second-order derivative absorption spectrum for $CsPbBr_3$, excitation spectrum, two-dimensional TRES in nanosecond time scale, normalized TA spectra at low and high fluence, PL decay obtained from the TCSPC technique, bleaching dynamics normalized at 1000 ps at low fluence and high fluence, biexciton Auger recombination lifetime measured by TAS and FLUPS, two-dimensional FLUPS spectra, DAS of $CsPbBr_3$ CNPls obtained by FLUPS at different fluences (PDF)

■ AUTHOR INFORMATION

Corresponding Author

*E-mail: je.moser@epfl.ch (J.-E.M.).

ORCID

Marco A. Schiavon: 0000-0002-1553-5388

Jacques-E. Moser: 0000-0003-0747-4666

Notes

The authors declare no competing financial interest.

■ ACKNOWLEDGMENTS

Financial support by the Swiss National Science Foundation; NCCR-MUST, a research instrument of the Swiss NSF; the Swiss Confederation through a Swiss Government Excellence Scholarship; and the Federal University of São João del-Rei is gratefully acknowledged. E.S. and J.E.M. are also very grateful to Nikolaus P. Ernsting, Humboldt-Univ. Berlin, for setting up the FLUPS instrumentation.

■ REFERENCES

(1) Kojima, A.; Teshima, K.; Shirai, Y.; Miyasaka, T. Organometal Halide Perovskites as Visible-Light Sensitizers for Photovoltaic Cells. *J. Am. Chem. Soc.* **2009**, *131*, 6050−6051.

(2) Luo, D.; Su, R.; Zhang, W.; Gong, Q.; Zhu, R. Minimizing Non-Radiative Recombination Losses in Perovskite Solar Cells. *Nat. Rev. Mater.* **2019**, DOI: 10.1038/s41578-019-0151-y.

(3) Wang, N.; Cheng, L.; Ge, R.; Zhang, S.; Miao, Y.; Zou, W.; Yi, C.; Sun, Y.; Cao, Y.; Yang, R.; et al. Perovskite Light-Emitting Diodes Based on Solution- Processed Self-Organized Multiple Quantum Wells. *Nat. Photonics* **2016**, *10*, 699−704.

(4) Zhang, L.; Yang, X.; Jiang, Q.; Wang, P.; Yin, Z.; Zhang, X.; Tan, H.; Yang, Y. M.; Wei, M.; Sutherland, B. R.; et al. Ultra-Bright and Highly Efficient Inorganic Based Perovskite Light-Emitting Diodes. *Nat. Commun.* **2017**, *8*, 15640.

(5) Li, Z.; Moon, J.; Gharajeh, A.; Haroldson, R.; Hawkins, R.; Hu, W.; Zakhidov, A.; Gu, Q. Room-Temperature Continuous-Wave Operation of Organometal Halide Perovskite Lasers. *ACS Nano* **2018**, *12*, 10968−10976.

(6) Miao, J.; Zhang, F. Recent Progress on Highly Sensitive Perovskite Photodetectors. *J. Mater. Chem. C* **2019**, *7*, 1741−1791.
(7) Lin, Y.; Martin, J. S.; Sun, Y.; Zhu, D.; Yan, Y. Lead Halide Perovskites for Photocatalytic Organic Synthesis. *Nat. Commun.* **2019**, *10*, 2843−2853.
(8) Sun, S.; Yuan, D.; Xu, Y.; Wang, A.; Deng, Z. Ligand-Mediated Synthesis of Shape- Controlled Cesium Lead Halide Perovskite Nanocrystals via Reprecipitation Process at Room-Temperature. *ACS Nano* **2016**, *10*, 3648−3657.
(9) Liang, Z.; Zhao, S.; Xu, Z.; Qiao, B.; Song, P.; Gao, D.; Xu, X. Shape-Controlled Synthesis of All-Inorganic $CsPbBr_3$ Perovskite Nanocrystals with Bright Blue Emission. *ACS Appl. Mater. Interfaces* **2016**, *8*, 28824−28830.
(10) Chung, H.; Jung, S. Il; Kim, H. J.; Cha, W.; Sim, E.; Kim, D.; Koh, W. K.; Kim, J. Composition-Dependent Hot Carrier Relaxation Dynamics in Cesium Lead Halide ($CsPbX_3$, X = Br and I) Perovskite Nanocrystals. *Angew. Chem., Int. Ed.* **2017**, *56*, 4160−4164.
(11) Hintermayr, V. A.; Polavarapu, L.; Urban, A. S.; Feldmann, J. Accelerated Carrier Relaxation through Reduced Coulomb Screening in Two-Dimensional Halide Perovskite Nanoplatelets. *ACS Nano* **2018**, *12*, 10151−10158.
(12) Yang, J.; Wen, X.; Xia, H.; Sheng, R.; Ma, Q.; Kim, J.; Tapping, P.; Harada, T.; Kee, T. W.; Huang, F.; et al. Acoustic-Optical Phonon up-Conversion and Hot-Phonon Bottleneck in Lead-Halide Perovskites. *Nat. Commun.* **2017**, *8*, 14120−14128.
(13) Mondal, A.; Aneesh, J.; Ravi, V. K.; Sharma, R.; Mir, W. J.; Beard, M. C.; Nag, A.; Adarsh, K. V. Ultrafast Exciton Many-Body Interactions and Hot-Phonon Bottleneck in Colloidal Cesium Lead Halide Perovskite Nanocrystals. *Phys. Rev. B: Condens. Matter Mater. Phys.* **2018**, *98*, 115418−115425.
(14) Nagamine, G.; Rocha, J. O.; Bonato, L. G.; Nogueira, A. F.; Zaharieva, Z.; Watt, A. A. R.; Cruz, C. H. D. B.; Padilha, L. A. Two-Photon Absorption and Two-Photon Induced Gain in Perovskite Quantum Dots. *J. Phys. Chem. Lett.* **2018**, *9*, 3478−3484.
(15) Castañeda, J. A.; Nagamine, G.; Yassitepe, E.; Bonato, L. G.; Voznyy, O.; Hoogland, S.; Nogueira, A. F.; Sargent, E. H.; Cruz, C. H. B.; Padilha, L. A. Efficient Biexciton Interaction in Perovskite Quantum Dots under Weak and Strong Confinement. *ACS Nano* **2016**, *10*, 8603−8609.
(16) Mondal, N.; Samanta, A. Complete Ultrafast Charge Carrier Dynamics in Photo-Excited All-Inorganic Perovskite Nanocrystals ($CsPbX_3$). *Nanoscale* **2017**, *9*, 1878−1885.
(17) Wang, Y.; Zhi, M.; Chang, Y.; Zhang, J.; Chan, Y. Stable, Ultralow Threshold Amplified Spontaneous Emission from $CsPbBr_3$ Nanoparticles Exhibiting Trion Gain. *Nano Lett.* **2018**, *18*, 4976−4984.
(18) Chen, J.; Messing, M. E.; Zheng, K.; Pullerits, T. Cation-Dependent Hot Carrier Cooling in Halide Perovskite Nanocrystals. *J. Am. Chem. Soc.* **2019**, *141*, 3532−3540.
(19) Chen, J.; Zidek, K.; Chabera, P.; Liu, D.; Cheng, P.; Nuuttila, L.; Al-Marri, M. J.; Lehtivuori, H.; Messing, M. E.; Han, K.; et al. Size- and Wavelength-Dependent Two-Photon Absorption Cross- Section of CsPbBr 3 Perovskite Quantum Dots. *J. Phys. Chem. Lett.* **2017**, *8*, 2316−2321.
(20) Mondal, N.; De, A.; Samanta, A. Biexciton Generation and Dissociation Dynamics in Formamidinium- and Chloride-Doped Cesium Lead Iodide Perovskite Nanocrystals. *J. Phys. Chem. Lett.* **2018**, *9*, 3673−3679.
(21) Pan, J.; Sarmah, S. P.; Murali, B.; Dursun, I.; Peng, W.; Parida, M. R.; Liu, J.; Sinatra, L.; Alyami, N.; Zhao, C.; et al. Air-Stable Surface-Passivated Perovskite Quantum Dots for Ultra-Robust, Single and Two-Photon-Induced Amplified Spontaneous Emission. *J. Phys. Chem. Lett.* **2015**, *6*, 5027−5033.
(22) Rossi, D.; Wang, H.; Dong, Y.; Qiao, T.; Qian, X.; Son, D. H. Light-Induced Activation of Forbidden Exciton Transition in Strongly Confined Perovskite Quantum Dots. *ACS Nano* **2018**, *12*, 12436−12443.
(23) Li, Y.; Lai, R.; Luo, X.; Liu, X.; Ding, T.; Lu, X.; Wu, K. On the Absence of a Phonon Bottleneck in Strongly Confined $CsPbBr_3$ Perovskite Nanocrystals. *Chem. Sci.* **2019**, *10*, 5983−5989.
(24) Dong, Y.; Qiao, T.; Kim, D.; Parobek, D.; Rossi, D.; Son, D. H. Precise Control of Quantum Confinement in Cesium Lead Halide Perovskite Quantum Dots via Thermodynamic Equilibrium. *Nano Lett.* **2018**, *18*, 3716−3722.
(25) Zhao, L.; Lustres, L. P.; Farztdinov, V.; Ernsting, N. Femtosecond Fluorescence Spectroscopy by Upconversion with Tilted Gate Pulses. *Phys. Chem. Chem. Phys.* **2005**, *7*, 1716−1725.
(26) Peng, L.; Geng, J.; Ai, L.; Zhang, Y.; Xie, R.; Yang, W. Room Temperature Synthesis of Ultra-Small, near-Unity Single-Sized Lead Halide Perovskite Quantum Dots with Wide Color Emission Tunability, High Color Purity and High Brightness. *Nanotechnology* **2016**, *27*, 335604.
(27) Akkerman, Q. A.; Motti, S. G.; Ram, A.; Kandada, S.; Mosconi, E.; Innocenzo, V. D.; Bertoni, G.; Marras, S.; Kamino, B. A.; Miranda, L.; et al. Solution Synthesis Approach to Colloidal Cesium Lead Halide Perovskite Nanoplatelets with Monolayer-Level Thickness Control. *J. Am. Chem. Soc.* **2016**, *138*, 1010−1016.
(28) Li, Q.; Lian, T. Ultrafast Charge Separation in Two-Dimensional $CsPbBr_3$ Perovskite Nanoplatelets. *J. Phys. Chem. Lett.* **2019**, *10*, 566−573.
(29) Li, J.; Gan, L.; Fang, Z.; He, H.; Ye, Z. Bright Tail States in Blue-Emitting Ultrasmall Perovskite Quantum Dots. *J. Phys. Chem. Lett.* **2017**, *8*, 6002−6008.
(30) Vitoreti, A. B. F.; Agouram, S.; De la Fuente, M.; Muñoz-Sanjosé, V.; Schiavon, M. A.; Mora-Seró, I. Study of the Partial Substitution of Pb by Sn in Cs-Pb-Sn-Br Nanocrystals Owing to Obtaining Stable Nanoparticles with Excellent Optical Properties. *J. Phys. Chem. C* **2018**, *122*, 14222−14231.
(31) Wu, Y.; Wei, C.; Li, X.; Li, Y.; Qiu, S.; Shen, W.; Cai, B.; Sun, Z.; Yang, D.; Deng, Z.; et al. In Situ Passivation of $PbBr_6^{4-}$ Octahedra toward Blue Luminescent $CsPbBr_3$ Nanoplatelets with Near 100% Absolute Quantum Yield. *ACS Energy Lett.* **2018**, *3*, 2030−2037.
(32) Li, J.; Luo, L.; Huang, H.; Ye, Z.; Zeng, J.; He, H. 2D Behaviors of Excitons in Cesium Lead Halide Perovskite Nanoplatelets. *J. Phys. Chem. Lett.* **2017**, *8*, 1161−1168.
(33) Protesescu, L.; Yakunin, S.; Bodnarchuk, M. I.; Krieg, F.; Caputo, R.; Hendon, C. H.; Yang, R. X.; Walsh, A.; Kovalenko, M. V. Nanocrystals of Cesium Lead Halide Perovskites ($CsPbX_3$, X = Cl, Br, and I): Novel Optoelectronic Materials Showing Bright Emission with Wide Color Gamut. *Nano Lett.* **2015**, *15*, 3692−3696.
(34) Grim, J. Q.; Christodoulou, S.; Stasio, F. Di; Krahne, R.; Cingolani, R. Continuous-Wave Biexciton Lasing at Room Temperature Using Solution-Processed Quantum Wells. *Nat. Nanotechnol.* **2014**, *9*, 891−895.
(35) Yang, Y.; Ostrowski, D. P.; France, R. M.; Zhu, K.; Van De Lagemaat, J.; Luther, J. M.; Beard, M. C. Observation of a Hot-Phonon Bottleneck in Lead-Iodide Perovskites. *Nat. Photonics* **2016**, *10*, 53−59.
(36) Mondal, N.; De, A.; Das, S.; Paul, S.; Samanta, A. Ultrafast Carrier Dynamics of Metal Halide Perovskite Nanocrystals and Perovskite. *Nanoscale* **2019**, *11*, 9796−9818.
(37) Makarov, N. S.; Guo, S.; Isaienko, O.; Liu, W.; Robel, I.; Klimov, V. I. Spectral and Dynamical Properties of Single Excitons, Biexcitons, and Trions in Cesium-Lead-Halide Perovskite Quantum Dots. *Nano Lett.* **2016**, *16* (4), 2349−2362.
(38) Li, Q.; Yang, Y.; Que, W.; Lian, T. Size and Morphology Dependent Auger Recombination in $CsPbBr_3$ Perovskite Two-Dimensional Nanoplatelets and One-Dimensional Nanorods. *Nano Lett.* **2019**, *19*, 5620−5627.
(39) Li, Y.; Ding, T.; Luo, X.; Chen, Z.; Liu, X.; Lu, X.; Wu, K. Biexciton Auger Recombination in Mono-Dispersed, Quantum-Confined $CsPbBr_3$ Perovskite Nanocrystals Obeys Universal Volume-Scaling. *Nano Res.* **2019**, *12*, 619−623.
(40) Padilha, L. A.; Stewart, J. T.; Sandberg, R. L.; Bae, W. K.; Koh, W.; Pietryga, M.; Klimov, V. I. Aspect Ratio Dependence of Auger

DOI: 10.1021/acs.jpclett.9b03282
J. Phys. Chem. Lett. 2020, 11, 387−394

Recombination and Carrier Multiplication in PbSe Nanorods. *Nano Lett.* **2013**, *13*, 1092−1099.
(41) Li, Q.; Lian, T. Area- and Thickness-Dependent Biexciton Auger Recombination in Colloidal CdSe Nanoplatelets: Breaking the " Universal Volume Scaling Law. *Nano Lett.* **2017**, *17*, 3152−3158.
(42) Klimov, V. I. Spectral and Dynamical Properties of Multiexcitons in Semiconductor Nanocrystals. *Annu. Rev. Phys. Chem.* **2007**, *58*, 635−673.
(43) Yumoto, G.; Tahara, H.; Kawawaki, T.; Saruyama, M.; Sato, R.; Teranishi, T.; Kanemitsu, Y. Hot Biexciton Effect on Optical Gain in $CsPbI_3$ Perovskite Nanocrystals. *J. Phys. Chem. Lett.* **2018**, *9*, 2222−2228.
(44) Aneesh, J.; Swarnkar, A.; Ravi, V. K.; Sharma, R.; Nag, A.; Adarsh, K. V. Ultrafast Exciton Dynamics in Colloidal $CsPbBr_3$ Perovskite Nanocrystals: Biexciton Effect and Auger Recombination. *J. Phys. Chem. C* **2017**, *121*, 4734−4739.
(45) Ashner, M. N.; Shulenberger, K. E.; Krieg, F.; Powers, E. R.; Kovalenko, M. V.; Bawendi, M. G.; Tisdale, W. A. Size-Dependent Biexciton Spectrum in $CsPbBr_3$ Perovskite Nanocrystals. *ACS Energy Lett.* **2019**, *4*, 2639−2645.
(46) Papagiorgis, P.; Protesescu, L.; Kovalenko, M. V.; Othonos, A.; Itskos, G. Long-Lived Hot Carriers in Formamidinium Lead Iodide Nanocrystals. *J. Phys. Chem. C* **2017**, *121*, 12434−12440.
(47) Papagiorgis, P.; Manoli, A.; Michael, S.; Bernasconi, C.; Bodnarchuk, M. I.; Kovalenko, M. V.; Othonos, A.; Itskos, G. Unraveling the Radiative Pathways of Hot Carriers upon Intense Photoexcitation of Lead Halide Perovskite Nanocrystals. *ACS Nano* **2019**, *13*, 5799−5809.

DOI: 10.1021/acs.jpclett.9b03282
J. Phys. Chem. Lett. 2020, 11, 387−394